The eag domain regulates hERG channel inactivation gating via a direct interaction

Ahleah S. Gustina[1,2] and Matthew C. Trudeau[2]

[1]Program in Neuroscience and [2]Department of Physiology, University of Maryland School of Medicine, Baltimore, MD 21201

Human ether-á-go-go (eag)-related gene (hERG) potassium channel kinetics are characterized by rapid inactivation upon depolarization, along with rapid recovery from inactivation and very slow closing (deactivation) upon repolarization. These factors combine to create a resurgent hERG current, where the current amplitude is paradoxically larger with repolarization than with depolarization. Previous data showed that the hERG N-terminal eag domain regulated deactivation kinetics by making a direct interaction with the C-terminal region of the channel. A primary mechanism for fast inactivation depends on residues in the channel pore; however, inactivation was also shown to be slower after deletion of a large N-terminal region. The mechanism for N-terminal region regulation of inactivation is unclear. Here, we investigated the contributions of the large N-terminal domains (amino acids 1–354), including the eag domain (amino acids 1–135), to hERG channel inactivation kinetics and steady-state inactivation properties. We found that N-deleted channels lacking just the eag domain (Δ2–135) or both the eag domain and the adjacent proximal domain (Δ2–354) had less rectifying current–voltage (I-V) relationships, slower inactivation, faster recovery from inactivation, and lessened steady-state inactivation. We coexpressed genetically encoded N-terminal fragments for the eag domain (N1–135) or the eag domain plus the proximal domain (N1–354) with N-deleted hERG Δ2–135 or hERG Δ2–354 channels and found that the resulting channels had more rectifying I-V relationships, faster inactivation, slower recovery from inactivation, and increased steady-state inactivation, similar to those properties measured for wild-type (WT) hERG. We also found that the eag domain–containing fragments regulated the time to peak and the voltage at the peak of a resurgent current elicited with a ramp voltage protocol. The eag domain–containing fragments effectively converted N-deleted channels into WT-like channels. Neither the addition of the proximal domain to the eag domain in N1–354 fragments nor the presence of the proximal domain in hERG Δ2–135 channels measurably affected inactivation properties; in contrast, the proximal region regulated steady-state activation in hERG Δ2–135 channels. The results show that N-terminal region-dependent regulation of channel inactivation and resurgent current properties are caused by a direct interaction of the eag domain with the rest of the hERG channel.

The Journal of General Physiology

INTRODUCTION

The human ether-á-go-go (eag)-related gene (hERG) encodes a voltage-activated potassium channel, which is a member of the eag channel family (Warmke and Ganetzky, 1994). hERG channels contribute to the repolarization of the ventricular action potential as the primary component of the cardiac delayed rectifier potassium current (I_{Kr}), and ERG channels have also been shown to modulate neuronal firing frequency (Sanguinetti and Jurkiewicz, 1990; Sanguinetti et al., 1995; Trudeau et al., 1995; Chiesa et al., 1997; Sacco et al., 2003; Pessia et al., 2008). Like other channels in the eag family, hERG has an eag domain, which comprises the first 135 amino acids of the N-terminal region (Morais Cabral et al., 1998). The eag domain contains a Per-Arnt-Sim (PAS) homology domain at amino acids 26–135 and a flexible N-terminal cap at amino acids 1–25 (Morais Cabral et al., 1998; Li et al., 2010; Muskett et al., 2011; Ng et al., 2011; Gustina and Trudeau, 2012). The eag domain is connected to the transmembrane domains of hERG by a long proximal domain (Viloria et al., 2000). The C-terminal region of hERG contains a cyclic nucleotide–binding homology domain (CNBHD), which is homologous to the cyclic nucleotide–binding domains in CNG and hyperpolarization-activated cyclic nucleotide–modulated channels (Warmke and Ganetzky, 1994; Zagotta et al., 2003; Brelidze et al., 2012); however, the hERG channel is not measurably regulated by direct binding of cyclic nucleotides (Brelidze et al., 2009).

hERG channel gating is characterized by slow closing (deactivation gating) (Sanguinetti et al., 1995; Trudeau et al., 1995). The N-terminal eag domain is a key modulator of slow deactivation gating (Spector et al., 1996;

Correspondence to Matthew C. Trudeau: mtrudeau@som.umaryland.edu

A.S. Gustina's present address is Dept. of Neuroscience, The Johns Hopkins University School of Medicine, Baltimore, MD 21205.

Abbreviations used in this paper: CFP, cyan fluorescent protein; CNBHD, cyclic nucleotide–binding homology domain; eag, ether-á-go-go; hERG, human eag-related gene; I_{Kr}, delayed rectifier potassium current; PAS, Per-Arnt-Sim.

The Rockefeller University Press $30.00
J. Gen. Physiol. Vol. 141 No. 2 229–241
www.jgp.org/cgi/doi/10.1085/jgp.201210870

Morais Cabral et al., 1998; Wang et al., 1998; Viloria et al., 2000; Gustina and Trudeau, 2009). Eag domains expressed as separate genetic fragments or peptides were shown to markedly regulate deactivation gating and to directly interact with intracellular regions of the hERG channel (Morais Cabral et al., 1998; Gustina and Trudeau, 2009, 2011; Fernández-Trillo et al., 2011; Trudeau et al., 2011). Importantly, eag domains expressed as genetic fragments do not interact with WT hERG channels, which indicates that these fragments are highly specific in their binding and regulatory function (Gustina and Trudeau, 2009; Gianulis and Trudeau, 2011). The C-terminal CNBHD also plays a role in the regulation of deactivation gating, as point mutations in the CNBHD (Al-Owais et al., 2009; Muskett et al., 2011) and deletions of the CNBHD (Gustina and Trudeau, 2011) speed deactivation gating. Furthermore, the CNBHD was shown to be necessary for eag domain modulation of deactivation gating and was shown to interact with the eag domain in biochemical pulldown assays, meaning that the eag domain and CNBHD directly interact to regulate deactivation gating (Gustina and Trudeau, 2011).

hERG channels also demonstrate a characteristic rectification in the I-V relationship, where the current conducted at negative potentials (in the range of −40 to 0 mV) is greater than the current conducted at positive potentials (20 to 80 mV) (Sanguinetti et al., 1995; Trudeau et al., 1995). Fast inactivation gating relative to slow activation gating has been implicated as the cause of hERG rectification (Schönherr and Heinemann, 1996; Smith et al., 1996; Spector et al., 1996; Herzberg et al., 1998). The primary mechanism for fast inactivation in hERG is thought to be similar to the C-type inactivation mechanism first described in Shaker K^+ channels (Hoshi et al., 1991; López-Barneo et al., 1993), because hERG inactivation is sensitive to external cations and mutations in the pore region (Schönherr and Heinemann, 1996; Smith et al., 1996; Herzberg et al., 1998). Channels with an N-terminal region deletion (hERG Δ2–354) had slower inactivation gating and reduced rectification compared with WT channels, indicating that the N-terminal regions were involved in modulation of inactivation; however, the mechanism for this regulation of inactivation is unclear (Spector et al., 1996; Wang et al., 1998).

In these studies, we investigated the role of the eag domain in regulation of hERG channel inactivation. We found that eag domain–containing fragments regulated inactivation rate, recovery from inactivation, and steady-state inactivation, indicating that direct protein interactions between the eag domain and the rest of the channel regulate inactivation properties of hERG channels. We also found that rectification was modulated directly by eag domains, as the peak of the I-V relationship was increased in channels lacking the eag domain, and was restored to smaller WT-like values by coexpression with eag domain–containing fragments. Finally, we administered a dynamic ramp protocol to investigate the hERG current profile under conditions more resembling a cardiac action potential. Under these conditions, the outward current from hERG gets bigger (resurges) with repolarization (Spector et al., 1996; Zhou et al., 1998; Sale et al., 2008) as a result of rapid recovery from inactivation and slow deactivation (Sale et al., 2008). We found that the time to peak of the current and the voltage at which the peak occurred in response to the voltage ramp were functions of the eag domain. Overall, our results show that the N-terminal eag domain is a determinant of hERG channel rectification, inactivation, and the peak and timing of the hERG resurgent current. In contrast, we found that the proximal N-terminal region did not measurably regulate inactivation properties, but rather regulated steady-state activation.

MATERIALS AND METHODS

Molecular biology

We previously generated and described the hERG, hERG ΔN, and N1–135 clones (Trudeau et al., 1995, 1999; Gustina and Trudeau, 2009). In this study, we constructed hERG Δeag and N1–354 using double overlap PCR. All channels and channel fragments used in this study were fused to fluorescent proteins. Citrine was fused directly to all hERG channels at the C terminus (after amino acid 1159), as in previous studies (Gustina and Trudeau, 2009). Monomeric enhanced cyan fluorescent protein (CFP) was fused directly at amino acid 135 (to make N1–135 CFP), as described previously (Gustina and Trudeau, 2009), and here, CFP was fused at position 354 (to make N1–354 CFP). All constructs were verified by standard fluorescence-based DNA sequencing. For expression in oocytes, mRNAs were made with the mMessage mMachine kit (Applied Biosystems).

Preparation and injection of oocytes

Xenopus laevis (Xenopus express) oocytes were collected from female frogs, as described previously (Gustina and Trudeau, 2011). Oocytes were pressure injected with 50.6 nl mRNA and incubated for 4–14 d at 16°C in ND96 with 50 µg/ml gentamicin (Sigma-Aldrich). For coexpression experiments, mRNA for the N-terminal region fragments was coinjected with mRNA for the transmembrane and C-terminal regions (Gustina and Trudeau, 2009). The ratio of fragments to channel RNA was empirically determined, and we used the ratio that resulted in maximal slowing of deactivation gating. This was usually a 2:1 ratio of fragment to channel. The total amount of mRNA injected remained constant.

Confocal microscopy

Fluorescent imaging was conducted using a confocal microscope (LSM5 Duo; Carl Zeiss) at the University of Maryland School of Medicine Facility for Confocal Microscopy. Cells were visualized using an inverted microscope (AxioObserver Z1; Carl Zeiss) with a 20×/NA1.0 water-immersion plan-apochromat objective. CFP and Citrine were excited using the 458- or 488-nm lines of an argon ion laser (Omnichrome), with emission captured at 475–525 or 505–550 nm, respectively. Fluorescence signals were collected from the animal pole of *Xenopus* oocytes after laser

excitation using acquisition software (Zen 2009; Carl Zeiss). Images were processed using the LSM Image Browser (Carl Zeiss) and Photoshop (CS5.1; Adobe).

Electrophysiology and analysis

Recordings from oocytes were performed as described previously (Gustina and Trudeau, 2009, 2011). In brief, recordings were made at room temperature, ~22–24°C, with a two-electrode voltage clamp (OC-725C; Warner Instruments) connected to an analogue to digital converter (ITC-18; InstruTech, Inc.). The external solution contained 4 mM KCl, 94 mM NaCl, 1 mM $MgCl_2$, 0.3 mM $CaCl_2$, and 5 mM HEPES, pH 7.4. Glass recording microelectrodes were filled with 3 M KCl and had resistances of 1–2 MΩ. Currents were recorded from a holding potential of −80 mV using Patchmaster software (HEKA) and were analyzed with Igor Pro software (WaveMetrics). We manually removed capacitance transients from all current traces to better visualize the data.

The I-V relationship was determined by normalizing peak outward current after 1-s depolarizations from −100 to +80 mV in 20-mV increments to the normalized extrapolated peak tail current at −100 mV. The extrapolated peak current value was determined from a single-exponential fit to the deactivating current extrapolated back to the time of the voltage change (Sale et al., 2008). To determine the steady-state activation (G-V) relationship we normalized the instantaneous tail currents at −50 mV (after 1-s steps from −100 to +40 mV in 20-mV increments) to the peak instantaneous tail current. G-V data were fit with a Boltzmann function ($y = 1/[1 + e^{[(V_{1/2} - V)/k]}]$). $V_{1/2}$ is the half-maximal activation potential, and k is the slope factor. Current relaxations with repolarizing voltage steps (deactivation) and the rising phase of the repolarizing voltage step (recovery from inactivation) were fit with an exponential function ($y = Ae^{(-t/\tau)}$) where t is time and τ is the time constant of deactivation or recovery from inactivation. The inactivation time constant was determined using a three-step protocol, as described previously, to isolate inactivating currents, which were fit with a single-exponential function (Spector et al., 1996; Herzberg et al., 1998; Wang et al., 1998). Steady-state inactivation was measured using a separate three-step protocol, as described previously (Smith et al., 1996). The equations $I_{corrected} = (g_{difference})(20 - E_{rev})$ and $g_{difference} = (I_{peak} - I_{end})/(E_{mem} - E_{rev})$ were used to correct errors in steady-state inactivation caused by deactivation at −120 and −100 mV. I_{peak} is the peak inward current during the conditioning pulse, and I_{end} is the inward current at the end of the conditioning pulse (Gianulis and Trudeau, 2011). The corrected peak instantaneous currents at 20 mV were normalized and fit with a Boltzmann function.

Data are presented as the mean ± SEM, where n represents the number of cells. Statistical analyses were performed using one-way ANOVA with a Newman–Keuls test for pairwise comparisons. A value of $P < 0.05$ was considered statistically significant.

Online supplemental material

As a negative control, we recorded currents from uninjected oocytes. We found that oocytes expressing hERG cRNA had robust

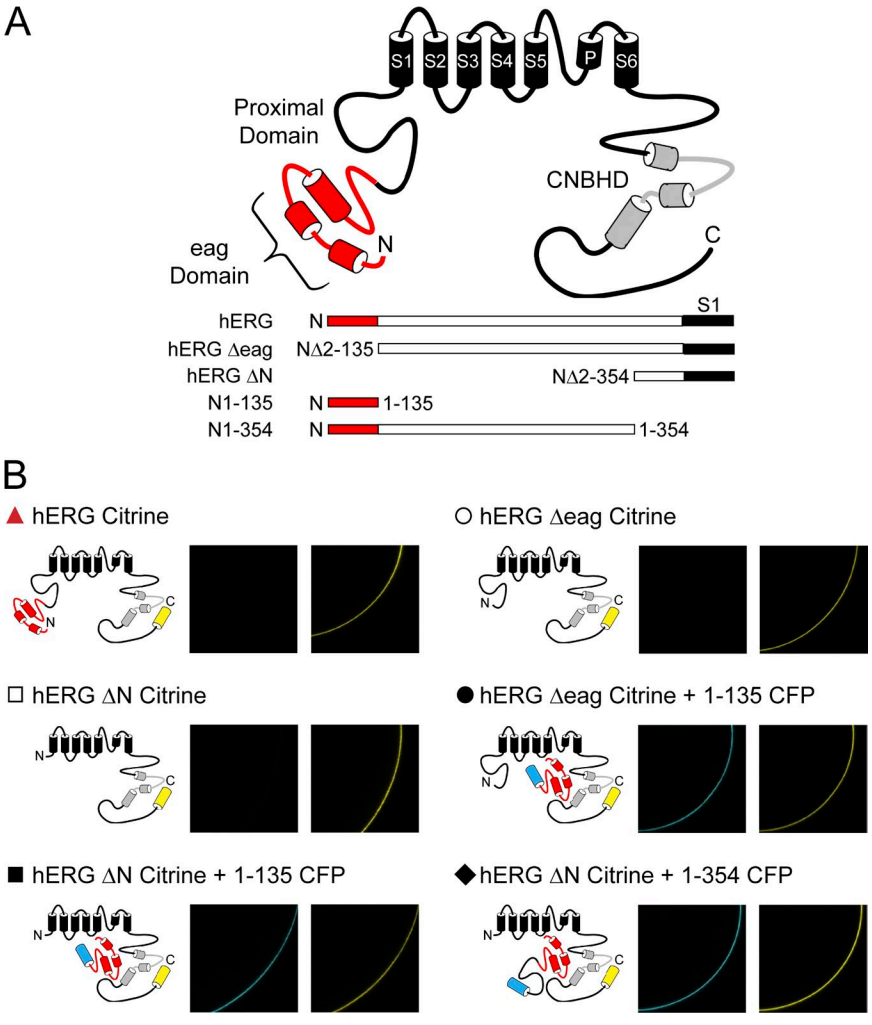

Figure 1. hERG channel schematic and confirmation of construct expression. (A) Schematic of hERG channel constructs used in this study. (B) Individual channel schematics and confocal images to confirm expression of all constructs. CFP (images on the left) was excited with a 458-nm argon ion laser, and emission was captured at 475–525 nm. Citrine (images on the right) was excited with a 488-nm argon ion laser, and emission was captured at 505–550 nm.

ionic currents in response to either a dynamic ramp or a series of voltage steps (Fig. S1, A and B), whereas uninjected oocytes had very small currents in response to the same voltage protocols (Fig. S1, C and D). Thus, endogenous oocyte currents were negligible and did not confound the measurement of hERG channel currents. Fig. S1 is available at http://www.jgp.org/cgi/content/full/jgp.201210870/DC1.

RESULTS

The eag domain is the primary regulator of deactivation gating, and the proximal domain does not measurably contribute to deactivation gating

To investigate the contributions of the N-terminal region eag domain and the adjacent proximal domain to hERG gating properties, we examined two hERG N-terminal region fragments of different lengths, one encoding the eag domain (amino acids 1–135; N1–135) and one encoding the eag domain and the proximal domain (amino acids 1–354; N1–354), and two different mutant hERG channels, one with a deletion of the eag domain (hERG Δ2–135 or hERG Δeag) and one with a deletion of the eag and proximal domains (hERGΔ2–354 or hERG ΔN) (Fig. 1 A). N-terminal region fragments were tagged with CFP at the C-terminal end, and all hERG channels were tagged with Citrine at the C-terminal end (see Materials and methods). Fragments and channels were expressed in oocytes, and expression was confirmed by confocal microscopy (Fig. 1 B). Currents were recorded using two-electrode voltage clamp. Channels were activated with a voltage step to 20 mV, followed by depolarizing pulses in 20-mV increments from −120 to −40 mV. We previously reported that a fragment encoding the N-terminal eag domain (N1–135) markedly regulated deactivation gating in hERG ΔN channels by making a direct interaction with the rest of the channel (Gustina and Trudeau 2009, 2011). In the previous experiments, neither the fragment nor the channel contained the proximal domain. Here, to evaluate the function of eag domains in the presence of proximal domains, we examined whether eag domains regulated channels with intact proximal domains (hERG Δeag), and then examined whether a fragment encoding the eag domain plus the proximal domain (N1–354) regulated deactivation gating in (hERG ΔN) channels that lacked these domains. As positive controls, we used WT hERG and hERG ΔN coexpressed with N1–135, in which the kinetics of deactivation were both slow (Fig. 2, A, C, and G). As a negative

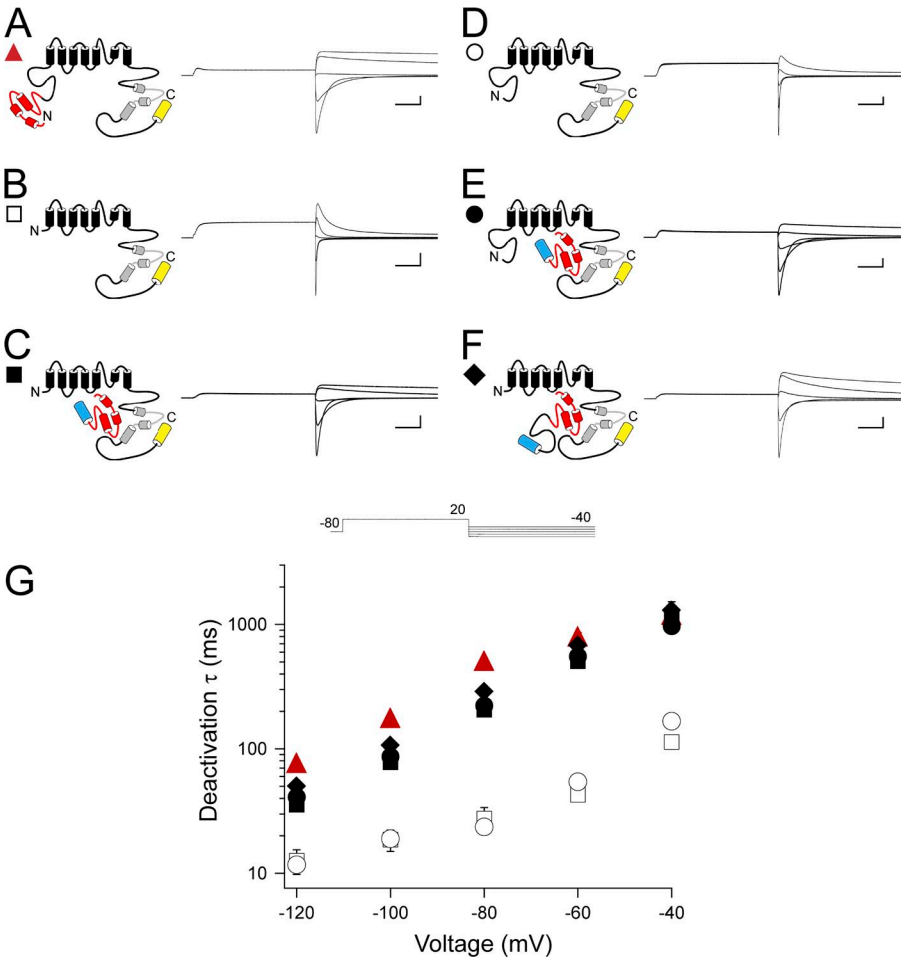

Figure 2. Regulation of deactivation gating by eag domains is unaffected by the presence of the proximal domain. (A–F) Channel schematics and two-electrode voltage-clamp recordings of tail currents from hERG (A), hERG ΔN (B), hERG ΔN plus N1–135 (C), hERG Δeag (D), hERG Δeag plus N1–135 (E), and hERG ΔN plus N1–354 (F). Currents were elicited using the pulse protocol shown. Calibration bars, 2 µA and 200 ms. (G) Plot of the time constants (τ) of deactivation derived from single-exponential fits (see Materials and methods) to the tail currents in A–F. Error bars are the SEM and are within the points if not visible. $n \geq 10$ for each construct.

control, we used hERG ΔN, in which the kinetics of deactivation were significantly faster ($P < 0.001$, ANOVA; Fig. 2, B and G). First, we found that channels lacking just the eag domain (hERG Δeag) had fast deactivation kinetics like the negative control, and that coexpression of hERG Δeag with N1–135 had significantly slower deactivation kinetics like the positive controls ($P < 0.001$, ANOVA; Fig. 2, D, E, and G). Second, we tested coexpression of hERG ΔN channels with the fragment encoding the eag domain plus proximal domain (N1–354) and found that these channels, like the positive controls, had slow deactivation kinetics, indicating that, like the eag domain fragment, the eag and proximal domain fragment significantly regulates deactivation gating ($P < 0.001$, ANOVA; Fig. 2, F and G). Collectively, these results indicate that the eag domain regulates channel deactivation, and that the proximal domain does not appear to contribute to or interfere with regulation of deactivation. These results support our previous findings that the eag domain is the primary determinant of deactivation gating, and that the proximal region does not play a measurable role in deactivation gating (Gustina and Trudeau, 2009, 2011).

Channels with N-terminal region deletions showed reduced inward rectification, which was recovered by coexpression of eag domain–containing fragments

To investigate the roles of the eag and proximal domains in hERG rectification properties, channels were activated by a series of pulses from −100 to +80 mV in 20-mV steps, followed by a repolarizing pulse to −100 mV. The steady-state I-V relationship was determined by taking the ratio of the peak outward current at the end of each depolarizing step to the extrapolated peak inward current at −100 mV (see Materials and methods). As anticipated, hERG channels exhibited a rectifying bell-shaped I-V relationship and had a relative peak outward current of 0.39 ± 0.05 at −20 mV (Fig. 3, A and G). hERG ΔN channels demonstrated reduced rectification, as indicated by a significant increase in the relative peak outward current at 0, 20, 40, and 60 mV compared with WT hERG, and a peak relative outward current of 0.73 ± 0.08 at 0 mV ($P < 0.001$, ANOVA; Fig. 3, B and G). Coexpression of hERG ΔN with N1–135 restored WT-like rectification properties, with a peak relative outward current of 0.23 ± 0.04 at −20 mV, which was not different from WT hERG (Fig. 3, C and G). Channels

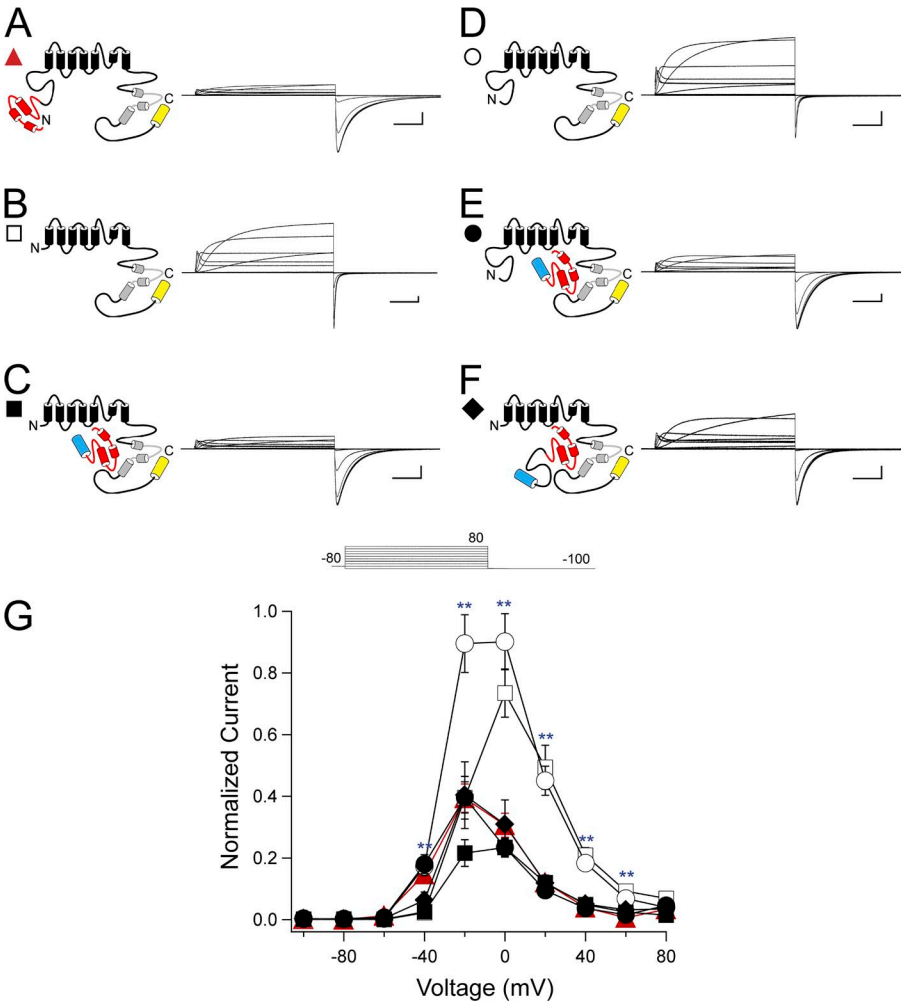

Figure 3. eag domain regulation of hERG rectification. (A–F) Channel schematics and two-electrode voltage-clamp recordings of a family of currents from hERG (A), hERG ΔN (B), hERG ΔN plus N1–135 (C), hERG Δeag (D), hERG Δeag plus N1–135 (E), and hERG ΔN plus N1–354 (F). Currents were elicited using the pulse protocol shown. Calibration bars, 1 µA and 200 ms. (G) Steady-state I-V curves derived from the currents shown in A–F by normalizing the peak outward current at the end of each depolarizing step to the extrapolated peak tail current at −100 mV and plotting versus voltage. Error bars are the SEM and are within the points if not visible. $n \geq 9$ for each construct. **, $P < 0.01$ versus hERG.

TABLE 1

Steady-state activation properties for hERG channels with N-terminal region deletions

Construct	$V_{1/2}$	*k*	*n*
	mV		
hERG	−27.87 ± 0.54	8.82 ± 0.12	11
hERG ΔN	−14.18 ± 1.31[a]	9.77 ± 0.53[b]	11
hERG ΔN + N1–135	−18.74 ± 0.64[a]	7.31 ± 0.18[a]	10
hERG Δeag	−27.19 ± 0.69	8.00 ± 0.25	10
hERG Δeag + N1–135	−31.88 ± 0.66[a]	8.19 ± 0.21	9
hERG ΔN + N1–354	−20.14 ± 0.87[a]	6.47 ± 0.25[a]	10

Boltzmann fit values for $V_{1/2}$ and slope (*k*). Values shown are the mean ± SEM; *n* indicates the number of cells.
[a]P < 0.01 versus HERG WT (ANOVA).
[b]P < 0.05 versus HERG WT (ANOVA).

with a deletion of just the eag domain, hERG Δeag, demonstrated significantly reduced rectification at −20, 0, 20, 40, and 60 mV compared with WT hERG, with a relative peak outward current of 0.90 ± 0.09 at 0 mV (P < 0.001, ANOVA; Fig. 3, D and G). Coexpression of hERG Δeag with N1–135 restored rectification to values not different from WT hERG at all voltages, with a relative peak outward current of 0.40 ± 0.05 at −20 mV (Fig. 2, E and G). hERG ΔN channels were then coexpressed with fragments encoding the full N-terminal region (N1–354). hERG ΔN plus N1–354 demonstrated restored WT-like rectification properties, with peak relative outward currents at −20 mV of 0.40 ± 0.11, which were not different from hERG at any voltage (Fig. 3, F and G). These results suggest that the eag domain was a determinant of channel rectification, as channels lacking most of the N-terminal region or lacking just the eag domain demonstrated reduced rectification, and coexpression of an eag domain–containing fragment restored rectification to levels similar to hERG. No significant differences were observed between hERG ΔN plus N1–135 and hERG ΔN plus N1–354, indicating no measurable effect of the proximal domain.

The proximal domain is involved in steady-state activation gating but may require a covalent link to the channel

We then measured steady-state activation by activating channels with a series of pulses from −100 to 40 mV, followed by a repolarizing pulse to −50 mV to elicit an outward tail current. The tail current after each voltage

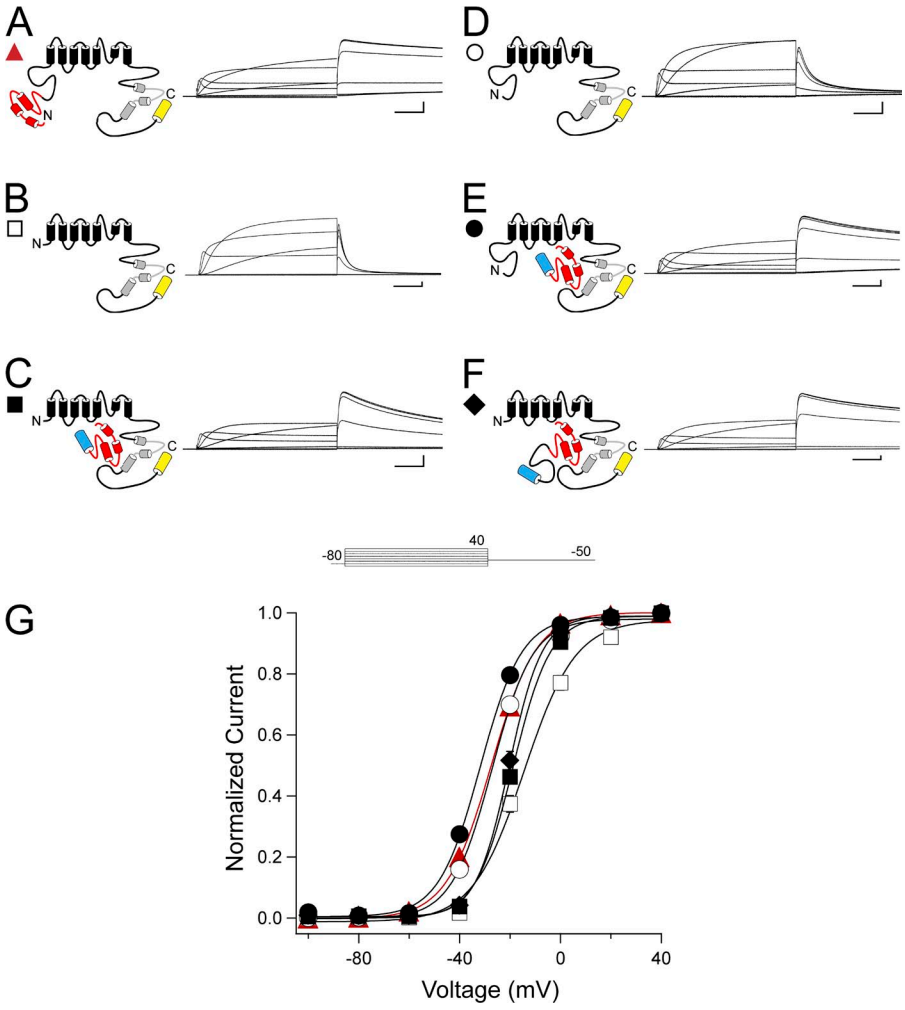

Figure 4. Proximal domain regulation of steady-state activation may require a covalent link to the channel. (A–F) Channel schematics and two-electrode voltage-clamp recordings of a family of currents from hERG (A), hERG ΔN (B), hERG ΔN plus N1–135 (C), hERG Δeag (D), hERG Δeag plus N1–135 (E), and hERG ΔN plus N1–354 (F). Currents were elicited using the pulse protocol shown. Calibration bars, 1 μA and 200 ms. (G) Steady-state activation (G-V) curves derived from the currents shown in A–F by normalizing the peak outward currents at −50 mV and plotting versus voltage. Data were fit with a Boltzmann function (see Materials and methods) to determine the $V_{1/2}$ and *k* (slope) values. Error bars are the SEM and are within the points if not visible. $n \geq 9$ for each construct.

step was normalized to the peak tail current. As reported previously, the steady-state activation curve for hERG ΔN is significantly right-shifted compared with hERG ($P < 0.001$, ANOVA; Fig. 4, A, B, and G, and Table 1) (Gustina and Trudeau, 2011). hERG ΔN coexpressed with N1–135 or N1–354 yielded a significant leftward shift and steeper slope compared with hERG ΔN alone, although these values were not recovered to the levels of hERG ($P < 0.001$, ANOVA; Fig. 3, C, F, and G, and Table 1). Interestingly, hERG Δeag and hERG Δeag plus N1–135 steady-state activation were not different from hERG (Fig. 3, D, E, and G, and Table 1). These data show that the right shift in steady-state activation only occurs when the proximal domain is deleted from the channel, and that deletion of the eag domain alone had no measurable effect on steady-state activation. Furthermore, hERG ΔN channels do not show a full recovery of the shift in steady-state activation when coexpressed with N1–354. This finding suggests that the proximal domain expressed in a separate fragment is unable to have an effect on gating. We interpret this result to mean that the proximal domain may require a peptide bond to the rest of the channel to regulate steady-state activation.

Channels with N-terminal region deletions have altered inactivation properties, which were recovered by coexpression of eag domain–containing fragments

The rising phase of the tail currents from Fig. 2 was fit with a single-exponential equation to determine the rate of recovery from inactivation (Sanguinetti et al., 1995). hERG had a significantly slower rate of recovery than hERG ΔN ($P < 0.001$, ANOVA; Fig. 5). hERG Δeag channels had fast recovery from inactivation, which was not different from hERG ΔN, whereas N-terminal region–deleted channels coexpressed with an eag domain–containing fragment (hERG Δeag plus N1–135 or hERG ΔN plus N1–354) had significantly slowed recovery from inactivation that was not different from that of hERG ($P < 0.001$, ANOVA; Fig. 5). These data suggest that a direct interaction between the eag domain and the rest of the channel regulates recovery from inactivation.

We next used a three-step protocol to isolate inactivating currents and determine the kinetics of inactivation (Smith et al., 1996; Spector et al., 1996; Herzberg et al., 1998; Wang et al., 1998). Channels were activated with a pulse to 20 mV, and then briefly stepped to −100 mV to allow the channels to recover from inactivation. The duration of the pulse to −100 mV was varied based on the rates of recovery from inactivation to prevent channels from deactivating during this step. We used a 20-ms pulse for hERG and N-terminal region–deleted channels coexpressed with an eag-containing fragment, and a 5-ms pulse for hERG ΔN and hERG Δeag channels. After the −100-mV pulse, steps were given in 10-mV increments between 0 and 60 mV to isolate the inactivating current. A single-exponential fit to the current decay was used to determine the time constant of inactivation. hERG channels demonstrated a consistent decrease in inactivation time constant as voltages became more positive, indicating a faster rate of inactivation at depolarized voltages (Fig. 6, A and D). hERG ΔN also demonstrated a progressive decrease in the time constant of inactivation with increasing voltages; however, the time constant of inactivation was significantly slower than hERG at all potentials, which is consistent with previous reports ($P < 0.001$, ANOVA; Fig. 6, B and D) (Spector et al., 1996). When hERG ΔN was coexpressed with N1–135, the inactivation time constant was restored to values not different from that of hERG at all

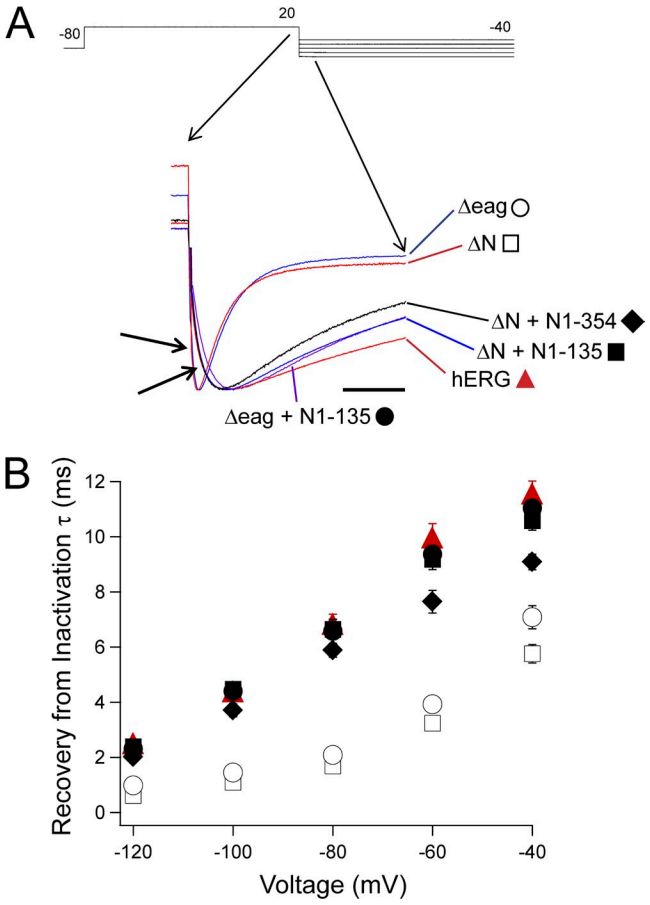

Figure 5. eag domain regulation of hERG recovery from inactivation. (A) Two-electrode voltage-clamp recordings of tail currents from the constructs indicated, enlarged to show the rising phase at the step to −100 mV. Currents were normalized to the peak for comparison. Calibration bar, 50 ms. (B) Plot of the time constants (τ) of recovery from inactivation derived from single-exponential fits to the rising phase of the tail currents in A from hERG (red triangle), hERG ΔN (open square), hERG ΔN plus N1–135 (closed square), hERG Δeag (open circle), hERG Δeag plus N1–135 (closed circle), and hERG ΔN plus N1–354 (closed diamond). Error bars are the SEM and are within the points if not visible. $n \geq 9$ for each construct.

voltages, suggesting a regulatory role for the eag domain in inactivation kinetics (Fig. 6, C and D). This role was further supported by hERG Δeag channels, which exhibited a rate of inactivation that was not different from hERG ΔN, and which was significantly slower than hERG at all potentials ($P < 0.01$, ANOVA; Fig. 6 D). Other constructs that were coexpressed with an eag-containing fragment (hERG Δeag plus N1–135 and hERG ΔN plus N1–354) were not different from hERG at any voltage and had a consistent decrease in the inactivation time constant (Fig. 6 D). Collectively, these results show that inactivation is not measurably regulated by the proximal domain, but rather inactivation kinetics are regulated directly by eag domains.

We then investigated the steady-state inactivation properties of hERG using a three-pulse protocol to isolate the peak instantaneous current (Fig. 7, arrows) (Smith et al., 1996). A depolarizing pulse to 20 mV was given to activate channels, followed by a step from −120 to 60 mV in 20-mV increments, and then a return to 20 mV. The duration of the voltage step from −120 to 60 mV was varied to allow the channels to recover from inactivation but not deactivate, based on the recovery from the inactivation rate of the channels (20-ms pulse for hERG, hERG ΔN plus N1–135, hERG Δeag plus N1–135, and hERG ΔN plus N1–354; 5-ms pulse for hERG ΔN and hERG Δeag). The peak instantaneous current was corrected to compensate for the small amount of deactivation that was detected at −100 or −120 mV (see Materials and methods). The steady-state inactivation curve for hERG ΔN had a $V_{1/2}$ of −59.60 ± 0.73 mV and a k (slope value) of 25.72 ± 0.32, which was significantly shallower and right-shifted compared with the $V_{1/2}$ of −68.69 ± 2.24 mV and a k of 19.51 ± 0.50 measured for hERG ($P < 0.05$, ANOVA; Fig. 7, A, B, and D, and Table 2). Coexpression of hERG ΔN plus N1–135 restored WT-like properties, with a $V_{1/2}$ of −74.15 ± 1.67 mV and a k of 19.51 ± 0.34, indicating a specific role for the eag domain in regulation of steady-state inactivation (Fig. 7, C and D, and Table 2). Consistent with this proposed role, other N-terminal region–deleted channels that were coexpressed with eag-containing fragments (hERG Δeag plus N1–135 and hERG ΔN plus N1–354) exhibited steady-state inactivation properties that were also not different from that of WT hERG (Fig. 7 D and Table 2). Channels lacking only the eag domain, hERG Δeag, however, had a $V_{1/2}$ of −60.97 ± 1.65 mV and a k of 24.74 ± 0.56, which was significantly shallower and right-shifted compared with WT, and was not different from that of hERG ΔN ($P < 0.05$, ANOVA; Fig. 7 D and Table 2). Collectively, these results show that the proximal domain did not play a measurable role in steady-state inactivation, whereas the eag domain regulated steady-state inactivation by a direct interaction with the rest of the channel.

The eag domain determines the timing of the peak hERG resurgent current

To investigate the role of N-terminal regions under conditions that mimic a cardiac ventricular action potential, we administered a dynamic ramp protocol by depolarizing cells to 0 mV for 200 ms, followed by a gradual decrease in the voltage to −100 mV over 200 ms before returning to the resting potential of −80 mV. The currents elicited for each cell were normalized to the extrapolated peak tail current at −100 mV after a 20-mV depolarization (see Materials and methods). A resurgent current characteristic of hERG, where the

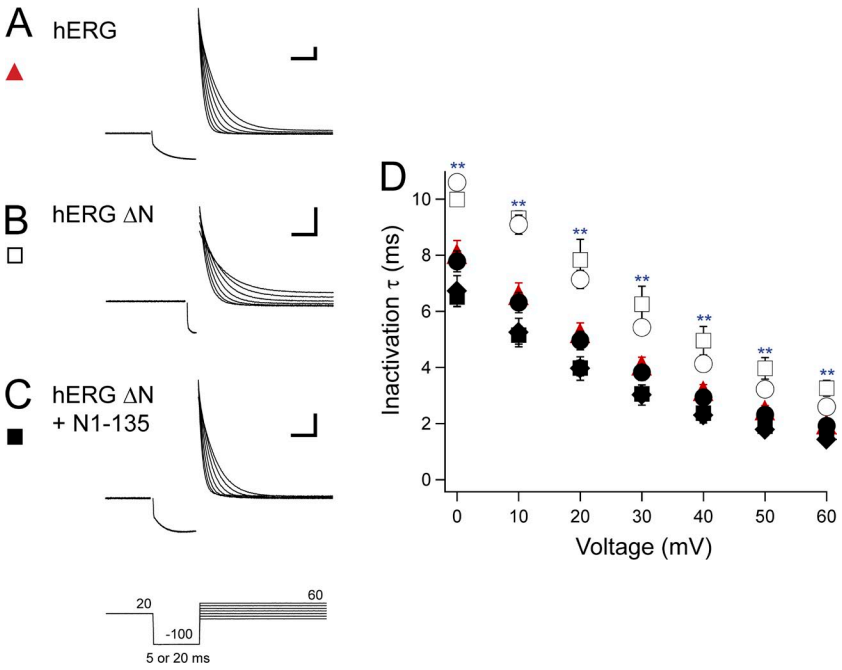

Figure 6. eag domain regulation of hERG inactivation rate. (A–C) Sample two-electrode voltage-clamp recordings to isolate inactivating currents from hERG (A), hERG ΔN (B), and hERG ΔN plus N1–135 (C) using the three-pulse protocol shown. The duration of the second pulse was 20 or 5 ms based on the construct so that minimal deactivation occurred during this step. Calibration bar, 2 μA and 10 ms. (D) Plot of the time constants (τ) of inactivation derived from single-exponential fits to the current decay in A–C and from hERG Δeag (open circle), hERG Δeag plus N1–135 (closed circle), and hERG ΔN plus N1–354 (closed diamond). Error bars are the SEM and are within the points if not visible. $n \geq 9$ for each construct. **, $P < 0.01$ versus hERG.

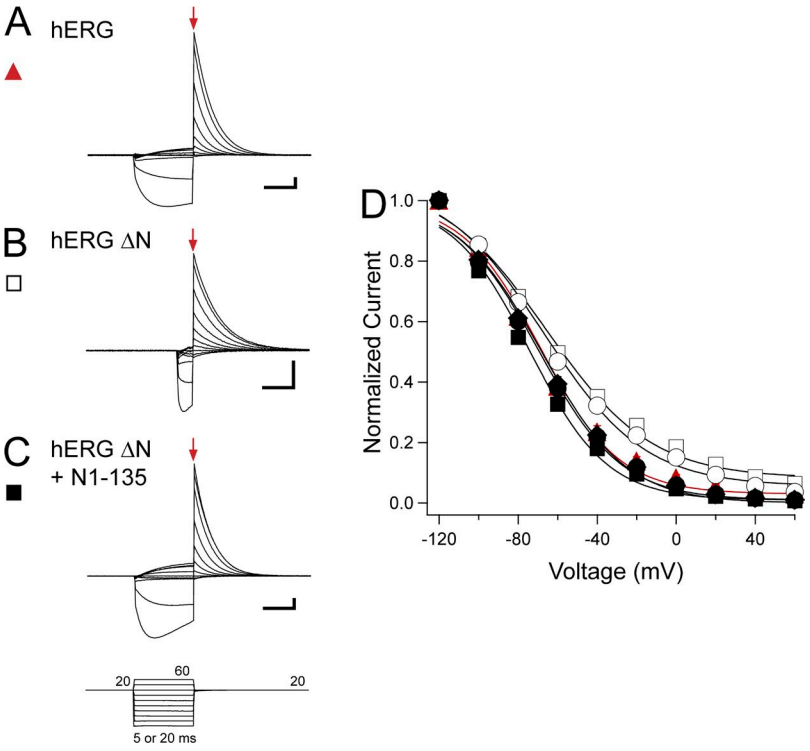

Figure 7. eag domain regulation of hERG steady-state inactivation. (A–C) Sample two-electrode voltage-clamp recordings from hERG (A), hERG ΔN (B), and hERG ΔN plus N1–135 (C) using the three-pulse protocol shown. The duration of the second pulse was 20 or 5 ms based on the construct. Red arrows indicate the peak instantaneous current. Calibration bar, 2 µA and 10 ms. (D) Steady-state inactivation curves derived from the currents shown in A–C and from hERG Δeag (open circle), hERG Δeag plus N1–135 (closed circle), and hERG ΔN plus N1–354 (closed diamond) by normalizing the peak instantaneous current and plotting versus voltage (see Materials and methods). Data were fit with a Boltzmann function to determine the $V_{1/2}$ and k (slope) values. Error bars are the SEM and are within the points if not visible. $n \geq 8$ for each construct.

peak current during the repolarizing ramp was greater than the peak current during the depolarizing step, was noted for all constructs tested (Fig. 8 A). The current peak for hERG occurs at an average voltage of −43 mV and 284 ms into the voltage command (Fig. 8, B–D). In contrast, hERG ΔN has a significantly earlier peak at an average voltage of −24 mV and 245 ms into the voltage command ($P < 0.001$, ANOVA; Fig. 8, B–D). The channel with just the eag domain deleted (hERG Δeag) had an earlier peak that was not different from that of hERG ΔN ($P < 0.01$, ANOVA; Fig. 8, B–D). N-terminal region–deleted channels that were coexpressed with an eag-containing fragment (hERG ΔN plus N1–135, hERG Δeag plus N1–135, and hERG ΔN plus N1–354) were not significantly different from hERG. hERG and N-terminal region–deleted channels coexpressed with N1–135 or N1–354 also demonstrated a large inward current at hyperpolarizing voltages, which was not seen in channels that lacked the eag domain ($P < 0.01$, ANOVA; Fig. 8, A, B, and E). These results suggest that the eag domain is a determinant of the timing and voltage dependence of the resurgent hERG current and the amplitude of the current undershoot at −100 mV.

DISCUSSION

Here we present evidence that the N-terminal eag domain is a determinant of hERG channel inactivation properties. We showed that, compared with WT channels, mutant channels with deletions of the eag domain or both the eag and proximal domains had faster deactivation, reduced rectification, slower inactivation, faster recovery from inactivation, and less steady-state inactivation. All of the kinetic or steady-state properties that were disrupted by deletion of the eag domain were recovered to levels similar to those in WT channels by coexpression of N-deleted channels with eag domain–containing gene fragments. Eag domains conferred N-deleted channels with slower deactivation, increased rectification, faster inactivation, slower recovery from inactivation, and more steady-state inactivation. Because the eag domain–containing gene fragments regulated inactivation parameters of N-deleted hERG channels, the eag domain regulates inactivation properties by directly interacting with the channel (Fig. 9).

TABLE 2

Steady-state inactivation properties for hERG channels with N-terminal region deletions

Construct	$V_{1/2}$	k	n
	mV		
hERG	−68.69 ± 2.24	19.51 ± 0.50	9
hERG ΔN	−59.60 ± 0.73[a]	25.72 ± 0.32[b]	8
hERG ΔN + N1–135	−74.15 ± 1.67	19.51 ± 0.34	10
hERG Δeag	−60.97 ± 1.65[a]	24.74 ± 0.56[b]	9
hERG Δeag + N1–135	−69.71 ± 1.70	20.35 ± 0.37	9
hERG ΔN + N1–354	−68.68 ± 2.35	20.49 ± 0.64	10

Boltzmann fit values for $V_{1/2}$ and slope (k). Values shown are the mean ± SEM; n indicates the number of cells.
[a]$P < 0.05$ versus HERG WT (ANOVA).
[b]$P < 0.01$ versus HERG WT (ANOVA).

How might the N-terminal eag domain regulate inactivation? There is a precedent for N-terminal regions influencing C-type inactivation in K^+ channels. For instance, in Shaker K^+ channels, an N-terminal peptide causes rapid N-type inactivation (Hoshi et al., 1990; Zagotta et al., 1990; Zhou et al., 2001) but also regulates the slower C-type inactivation as a secondary consequence of binding at the pore (Hoshi et al., 1991; Baukrowitz and Yellen, 1995). Like C-type inactivation in Shaker (Hoshi et al., 1991; López-Barneo et al., 1993), hERG inactivation is dependent on pore residues (Schönherr and Heinemann, 1996; Smith et al., 1996; Herzberg et al., 1998) and the S6 domain (Herzberg et al., 1998). But the short cap region of the eag domain does not appear to bind the pore (Wang et al., 2000). Instead, the eag domain interacts stably with the C-terminal CNBHD (Gustina and Trudeau, 2011). Interestingly, point mutations in the PAS region of the eag domain alter deactivation and inactivation (Chen et al., 1999; Gianulis and Trudeau, 2011), whereas deletion of the cap region altered deactivation but not inactivation (Wang et al., 1998). An interpretation of these results is that the PAS domain region but not the cap region of the eag domain is necessary for regulating inactivation. To explain all of these findings, we propose that the direct association of the eag domain with the CNBHD is communicated to residues in the S6 that influence C-type inactivation.

To isolate inactivation kinetics and generate steady-state inactivation curves, we used longer duration pulses (20 ms) for WT channels and N-deleted channels coinjected with eag domain–containing fragments and shorter duration pulses (5 ms) for N-deleted channels during the second pulse of three-pulse protocols (Figs. 6 and 7). The 20-ms second pulse in eag domain–containing channels was necessary to isolate open channels that had fully recovered from inactivation. The 5-ms second pulse in N-deleted channel recordings was

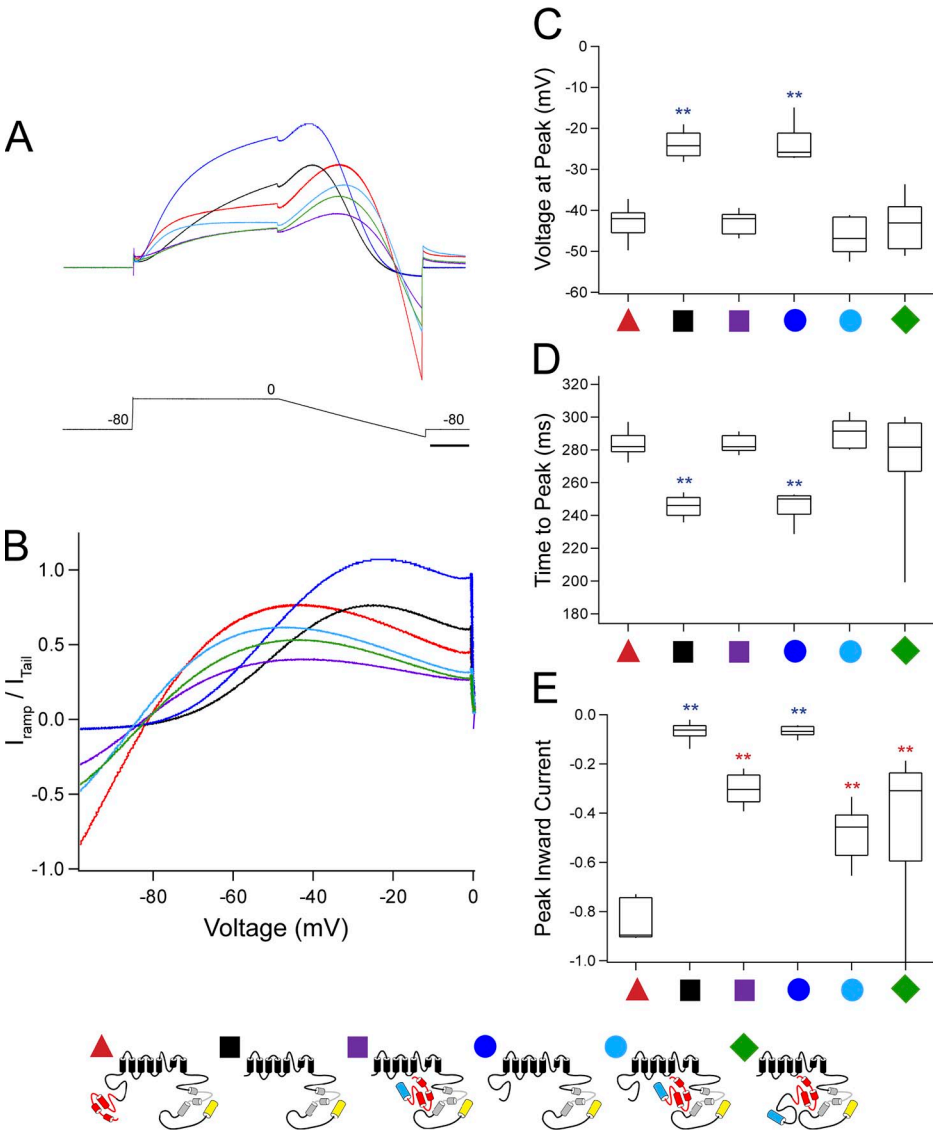

Figure 8. The eag domain regulates the timing of the peak hERG resurgent current. (A) Representative current recordings of hERG (red), hERG ΔN (black), hERG ΔN plus N1–135 (purple), hERG Δeag (blue), hERG Δeag plus N1–135 (light blue), and hERG ΔN plus N1–354 (green) in response to a dynamic ramp clamp. Currents were normalized to the extrapolated peak tail at −100 mV (see Materials and methods). Bar, 50 ms. (B) Graph of the normalized current from A versus the voltage during the current ramp. (C) Box plot of the voltage at the current peak in A and B for the constructs indicated. (D) Box plot of the time to the current peak in A and B for the constructs indicated. (E) Box plot of the peak inward current at −100 mV derived from A and B for the constructs indicated. The middle line of the box is the mean, the top and bottom are the 75th and 25th percentiles, and the vertical lines indicate the 90th and 10th percentiles. $n \geq 10$ for each construct. **, $P < 0.01$ versus hERG and versus hERG and hERG ΔN.

necessary to isolate open channels at negative voltages before they rapidly closed (as a result of the lack of the eag domain). If the second pulse was lengthened for N-deleted channels, the channels deactivated rapidly and were not available for measuring inactivation. Although necessary, comparing data using two different second-pulse durations was not ideal because the N-deleted channels and channels with eag domains were equilibrating between open and inactive states for different periods of time. The shorter equilibration times of N-deleted channels, combined with the larger time constant of inactivation in these channels, means that the steady-state inactivation curves may be less right-shifted in N-deleted channels, and with less of a change in slope, than if the channels were allowed to equilibrate for 20 ms. However, it is clear from examining the inactivating currents in Fig. 6 that the hERG ΔN channel currents reach a new steady-state level a the end of the third pulse compared with WT hERG or hERG ΔN plus N1–135 channels (see Fig. 6, A–C), meaning that the channels reach less of a steady-state level of inactivation than WT channels. The larger peak currents in the I-V plots of N-deleted channels compared with WT channels also suggests a change in steady-state inactivation (Fig. 3 G).

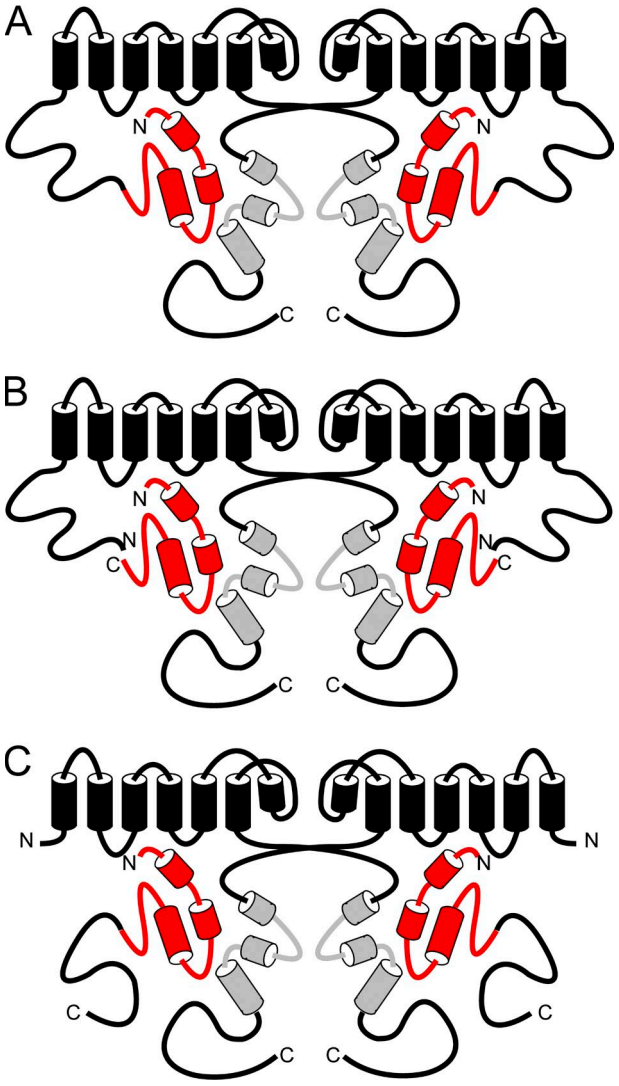

Figure 9. Model of eag domain interaction with the channel. (A) Schematic of WT hERG showing eag domain interaction with the CNBHD and a proximal domain, which is continuous with the transmembrane regions. (B) Schematic of hERG Δeag plus N1–135 showing eag domain interaction with the CNBHD and a proximal domain, which is continuous with the transmembrane regions but not attached to the eag domain. (C) Schematic of hERG ΔN plus N1–354 showing eag domain interaction with the CNBHD and a proximal domain, which is continuous with the eag domain but not connected to the transmembrane regions.

We found that the hERG proximal N-terminal region regulated steady-state activation under certain configurations. Our data showed that hERG Δeag channels, which had intact proximal domains, had steady-state activation that was not different from that of WT channels. However, hERG ΔN channels, which lack the proximal domain, had right-shifted steady-state activation, suggesting that steady-state activation was regulated by the proximal domain, but not the eag domain. The WT-like $V_{1/2}$ of steady-state activation was not recovered by coexpression of hERG ΔN with N1–354, a proximal domain–containing fragment, although this fragment was able to interact with the channel, as indicated by its modulation of rectification and inactivation properties. One possible explanation for this result is that the proximal domain polypeptide is unable to modulate steady-state activation as a result of an inability to interact with the channel, even when attached to an eag domain that was able to interact with the rest of the channel (Fig. 9 C). Our data suggest that, in order for the proximal domain to regulate steady-state activation, it must be covalently linked to the remaining N-terminal residues. These residues include a charge cluster (KIKER; amino acids 362–366) near the S1 transmembrane domain, which was previously shown to be involved in regulation of hERG steady-state activation (Viloria et al., 2000; Saenen et al., 2006). Perhaps the proximal domain modulates gating through an interaction with the KIKER charge cluster, which is disrupted when the domain is not covalently attached to the channel.

We conducted experiments with a dynamic ramp clamp, which was designed to replicate some of the voltage changes during a cardiac action potential, including the depolarization and plateau phase, followed by a repolarization phase (Spector et al., 1996; Chen et al., 1999; Gianulis and Trudeau, 2011). Our experiments showed that the time to peak of the current was shorter and occurred at a more positive voltage in channels lacking the eag domain. Channels lacking the eag domain also had only a small inward current at −100 mV compared with that observed in WT channels. The shifts

in time to peak, voltage dependence, and inward current at −100 mV were recovered by coexpression of N-deleted channels with eag domain–containing fragments. These results indicate that the direct interaction of the eag domain with the channel is a key determinant of the timing of the resurgent hERG current.

Our results provide a mechanistic explanation for how a native N-terminal–deleted hERG subunit (hERG1b) regulates the timing of resurgent hERG currents. ERG1b is a naturally occurring isoform that has an N-terminal region composed of only 59 amino acids and lacks an eag domain (Lees-Miller et al., 1997; London et al., 1997). Along with mammalian ERG1a subunits, native ERG1b subunits form the I_{Kr} current in native cardiomyocytes (Lees-Miller et al., 1997; London et al., 1997; Jones et al., 2004), where the resurgent I_{Kr} current is thought to be critical for repolarization (Sanguinetti and Jurkiewicz, 1990; Zhou et al., 1998; Sale et al., 2008). Entirely consistent with channels lacking an eag domain, mammalian ERG1b channels or heteromeric ERG1a/ERG1b channels have fast deactivation kinetics, less rectifying I-V relationships, and earlier time to peak of resurgent currents compared with ERG1a channels (Lees-Miller et al., 1997; London et al., 1997; Sale et al., 2008; Larsen and Olesen, 2010; Trudeau et al., 2011). Differential expression levels of ERG1a and ERG1b subunits may be a mechanism for modulation of peak resurgent current and thus the degree of action potential repolarization by I_{Kr}. The kinetic properties of hERG1b and the time to peak of resurgent currents in heteromeric hERG1a/hERG1b channels are directly regulated by eag domain polypeptides (Trudeau et al., 2011). Here, we show that eag domains directly regulate resurgent current time to peak in N-deleted (hERG ΔN or hERG Δeag) channels, meaning that (a) direct eag domain regulation of channel properties is independent of the novel hERG1b N-terminal region, and is instead a general property of channels that lack eag domains; and (b) the direct modulation of channels by eag domains may help to regulate the physiologically important resurgent I_{Kr} current.

A central mystery in hERG channel gating is how the eag domain regulates deactivation gating, inactivation gating, and steady-state inactivation properties. A major conclusion made possible by our finding that genetically encoded eag domain–containing fragments regulate inactivation is that direct protein interactions must underlie key steps in the regulation of inactivation gating. There is evidence that deletions of the cap region of the eag domain affect deactivation, but not inactivation, so protein interactions underlying deactivation and inactivation may be separable, which would lead to a better understanding of the two mechanisms. Protein interactions can be studied by numerous well-established methods, and these techniques may be used to understand eag domain interactions in more detail.

We thank L. Leung for preparation of oocytes and technical assistance.

This work was supported by a National Institutes of Health grant (HL-083121 to M.C. Trudeau), an American Heart Association Mid-Atlantic Affiliate Predoctoral Fellowship (to A.S. Gustina), and a gift from the Helen Pumphrey Denit Trust.

Kenton J. Swartz served as editor.

Submitted: 24 July 2012
Accepted: 27 December 2012

REFERENCES

Al-Owais, M., K. Bracey, and D. Wray. 2009. Role of intracellular domains in the function of the herg potassium channel. *Eur. Biophys. J.* 38:569–576. http://dx.doi.org/10.1007/s00249-009-0408-2

Baukrowitz, T., and G. Yellen. 1995. Modulation of K+ current by frequency and external [K+]: a tale of two inactivation mechanisms. *Neuron.* 15:951–960. http://dx.doi.org/10.1016/0896-6273(95)90185-X

Brelidze, T.I., A.E. Carlson, and W.N. Zagotta. 2009. Absence of direct cyclic nucleotide modulation of mEAG1 and hERG1 channels revealed with fluorescence and electrophysiological methods. *J. Biol. Chem.* 284:27989–27997. http://dx.doi.org/10.1074/jbc.M109.016337

Brelidze, T.I., A.E. Carlson, B. Sankaran, and W.N. Zagotta. 2012. Structure of the carboxy-terminal region of a KCNH channel. *Nature.* 481:530–533. http://dx.doi.org/10.1038/nature10735

Chen, J., A. Zou, I. Splawski, M.T. Keating, and M.C. Sanguinetti. 1999. Long QT syndrome-associated mutations in the Per-Arnt-Sim (PAS) domain of HERG potassium channels accelerate channel deactivation. *J. Biol. Chem.* 274:10113–10118. http://dx.doi.org/10.1074/jbc.274.15.10113

Chiesa, N., B. Rosati, A. Arcangeli, M. Olivotto, and E. Wanke. 1997. A novel role for HERG K+ channels: spike-frequency adaptation. *J. Physiol.* 501:313–318. (published erratum appears in *J. Physiol. (Lond).* 1997. 502:715) http://dx.doi.org/10.1111/j.1469-7793.1997.313bn.x

Fernández-Trillo, J., F. Barros, A. Machín, L. Carretero, P. Domínguez, and P. de la Peña. 2011. Molecular determinants of interactions between the N-terminal domain and the transmembrane core that modulate hERG K+ channel gating. *PLoS ONE.* 6:e24674. http://dx.doi.org/10.1371/journal.pone.0024674

Gianulis, E.C., and M.C. Trudeau. 2011. Rescue of aberrant gating by a genetically encoded PAS (Per-Arnt-Sim) domain in several long QT syndrome mutant human ether-á-go-go-related gene potassium channels. *J. Biol. Chem.* 286:22160–22169. http://dx.doi.org/10.1074/jbc.M110.205948

Gustina, A.S., and M.C. Trudeau. 2009. A recombinant N-terminal domain fully restores deactivation gating in N-truncated and long QT syndrome mutant hERG potassium channels. *Proc. Natl. Acad. Sci. USA.* 106:13082–13087. http://dx.doi.org/10.1073/pnas.0900180106

Gustina, A.S., and M.C. Trudeau. 2011. hERG potassium channel gating is mediated by N- and C-terminal region interactions. *J. Gen. Physiol.* 137:315–325. http://dx.doi.org/10.1085/jgp.201010582

Gustina, A.S., and M.C. Trudeau. 2012. HERG potassium channel regulation by the N-terminal eag domain. *Cell. Signal.* 24:1592–1598. http://dx.doi.org/10.1016/j.cellsig.2012.04.004

Herzberg, I.M., M.C. Trudeau, and G.A. Robertson. 1998. Transfer of rapid inactivation and sensitivity to the class III antiarrhythmic drug E-4031 from HERG to M-eag channels. *J. Physiol.* 511:3–14. http://dx.doi.org/10.1111/j.1469-7793.1998.003bi.x

Hoshi, T., W.N. Zagotta, and R.W. Aldrich. 1990. Biophysical and molecular mechanisms of Shaker potassium channel inactivation. *Science.* 250:533–538. http://dx.doi.org/10.1126/science.2122519

Hoshi, T., W.N. Zagotta, and R.W. Aldrich. 1991. Two types of inactivation in Shaker K+ channels: effects of alterations in the carboxy-terminal region. *Neuron.* 7:547–556. http://dx.doi.org/10.1016/0896-6273(91)90367-9

Jones, E.M., E.C. Roti Roti, J. Wang, S.A. Delfosse, and G.A. Robertson. 2004. Cardiac IKr channels minimally comprise hERG 1a and 1b subunits. *J. Biol. Chem.* 279:44690–44694. http://dx.doi.org/10.1074/jbc.M408344200

Larsen, A.P., and S.-P. Olesen. 2010. Differential expression of hERG1 channel isoforms reproduces properties of native I(Kr) and modulates cardiac action potential characteristics. *PLoS ONE.* 5:e9021. http://dx.doi.org/10.1371/journal.pone.0009021

Lees-Miller, J.P., C. Kondo, L. Wang, and H.J. Duff. 1997. Electrophysiological characterization of an alternatively processed ERG K+ channel in mouse and human hearts. *Circ. Res.* 81:719–726. http://dx.doi.org/10.1161/01.RES.81.5.719

Li, Q., S. Gayen, A.S. Chen, Q. Huang, M. Raida, and C. Kang. 2010. NMR solution structure of the N-terminal domain of hERG and its interaction with the S4-S5 linker. *Biochem. Biophys. Res. Commun.* 403:126–132. http://dx.doi.org/10.1016/j.bbrc.2010.10.132

London, B., M.C. Trudeau, K.P. Newton, A.K. Beyer, N.G. Copeland, D.J. Gilbert, N.A. Jenkins, C.A. Satler, and G.A. Robertson. 1997. Two isoforms of the mouse ether-a-go-go-related gene coassemble to form channels with properties similar to the rapidly activating component of the cardiac delayed rectifier K+ current. *Circ. Res.* 81:870–878. http://dx.doi.org/10.1161/01.RES.81.5.870

López-Barneo, J., T. Hoshi, S.H. Heinemann, and R.W. Aldrich. 1993. Effects of external cations and mutations in the pore region on C-type inactivation of Shaker potassium channels. *Receptors Channels.* 1:61–71.

Morais Cabral, J.H., A. Lee, S.L. Cohen, B.T. Chait, M. Li, and R. Mackinnon. 1998. Crystal structure and functional analysis of the HERG potassium channel N terminus: a eukaryotic PAS domain. *Cell.* 95:649–655. http://dx.doi.org/10.1016/S0092-8674(00)81635-9

Muskett, F.W., S. Thouta, S.J. Thomson, A. Bowen, P.J. Stansfeld, and J.S. Mitcheson. 2011. Mechanistic insight into human ether-à-go-go-related gene (hERG) K+ channel deactivation gating from the solution structure of the EAG domain. *J. Biol. Chem.* 286:6184–6191. http://dx.doi.org/10.1074/jbc.M110.199364

Ng, C.A., M.J. Hunter, M.D. Perry, M. Mobli, Y. Ke, P.W. Kuchel, G.F. King, D. Stock, and J.I. Vandenberg. 2011. The N-terminal tail of hERG contains an amphipathic α-helix that regulates channel deactivation. *PLoS ONE.* 6:e16191. http://dx.doi.org/10.1371/journal.pone.0016191

Pessia, M., I. Servettini, R. Panichi, L. Guasti, S. Grassi, A. Arcangeli, E. Wanke, and V.E. Pettorossi. 2008. ERG voltage-gated K+ channels regulate excitability and discharge dynamics of the medial vestibular nucleus neurones. *J. Physiol.* 586:4877–4890. http://dx.doi.org/10.1113/jphysiol.2008.155762

Sacco, T., A. Bruno, E. Wanke, and F. Tempia. 2003. Functional roles of an ERG current isolated in cerebellar Purkinje neurons. *J. Neurophysiol.* 90:1817–1828. http://dx.doi.org/10.1152/jn.00104.2003

Saenen, J.B., A.J. Labro, A. Raes, and D.J. Snyders. 2006. Modulation of HERG gating by a charge cluster in the N-terminal proximal domain. *Biophys. J.* 91:4381–4391. http://dx.doi.org/10.1529/biophysj.106.087247

Sale, H., J. Wang, T.J. O'Hara, D.J. Tester, P. Phartiyal, J.Q. He, Y. Rudy, M.J. Ackerman, and G.A. Robertson. 2008. Physiological properties of hERG 1a/1b heteromeric currents and a hERG 1b-specific mutation associated with Long-QT syndrome. *Circ. Res.* 103:e81–e95. http://dx.doi.org/10.1161/CIRCRESAHA.108.185249

Sanguinetti, M.C., and N.K. Jurkiewicz. 1990. Two components of cardiac delayed rectifier K^+ current. Differential sensitivity to block by class III antiarrhythmic agents. *J. Gen. Physiol.* 96:195–215. http://dx.doi.org/10.1085/jgp.96.1.195

Sanguinetti, M.C., C. Jiang, M.E. Curran, and M.T. Keating. 1995. A mechanistic link between an inherited and an acquired cardiac arrhythmia: HERG encodes the IKr potassium channel. *Cell.* 81:299–307. http://dx.doi.org/10.1016/0092-8674(95)90340-2

Schönherr, R., and S.H. Heinemann. 1996. Molecular determinants for activation and inactivation of HERG, a human inward rectifier potassium channel. *J. Physiol.* 493:635–642.

Smith, P.L., T. Baukrowitz, and G. Yellen. 1996. The inward rectification mechanism of the HERG cardiac potassium channel. *Nature.* 379:833–836. http://dx.doi.org/10.1038/379833a0

Spector, P.S., M.E. Curran, A. Zou, M.T. Keating, and M.C. Sanguinetti. 1996. Fast inactivation causes rectification of the I_{Kr} channel. *J. Gen. Physiol.* 107:611–619. http://dx.doi.org/10.1085/jgp.107.5.611

Trudeau, M.C., J.W. Warmke, B. Ganetzky, and G.A. Robertson. 1995. HERG, a human inward rectifier in the voltage-gated potassium channel family. *Science.* 269:92–95. http://dx.doi.org/10.1126/science.7604285

Trudeau, M.C., S.A. Titus, J.L. Branchaw, B. Ganetzky, and G.A. Robertson. 1999. Functional analysis of a mouse brain Elk-type K+ channel. *J. Neurosci.* 19:2906–2918.

Trudeau, M.C., L.M. Leung, E.R. Roti, and G.A. Robertson. 2011. hERG1a N-terminal eag domain–containing polypeptides regulate homomeric hERG1b and heteromeric hERG1a/hERG1b channels: A possible mechanism for long QT syndrome. *J. Gen. Physiol.* 138:581–592. http://dx.doi.org/10.1085/jgp.201110683

Viloria, C.G., F. Barros, T. Giráldez, D. Gómez-Varela, and P. de la Peña. 2000. Differential effects of amino-terminal distal and proximal domains in the regulation of human erg K(+) channel gating. *Biophys. J.* 79:231–246. http://dx.doi.org/10.1016/S0006-3495(00)76286-2

Wang, J., M.C. Trudeau, A.M. Zappia, and G.A. Robertson. 1998. Regulation of deactivation by an amino terminal domain in human ether-à-go-go–related gene potassium channels. *J. Gen. Physiol.* 112:637–647. (published erratum appears in *J. Gen. Physiol.* 1999. 113:359) http://dx.doi.org/10.1085/jgp.112.5.637

Wang, J., C.D. Myers, and G.A. Robertson. 2000. Dynamic control of deactivation gating by a soluble amino-terminal domain in *HERG* K^+ channels. *J. Gen. Physiol.* 115:749–758. http://dx.doi.org/10.1085/jgp.115.6.749

Warmke, J.W., and B. Ganetzky. 1994. A family of potassium channel genes related to eag in Drosophila and mammals. *Proc. Natl. Acad. Sci. USA.* 91:3438–3442. http://dx.doi.org/10.1073/pnas.91.8.3438

Zagotta, W.N., T. Hoshi, and R.W. Aldrich. 1990. Restoration of inactivation in mutants of Shaker potassium channels by a peptide derived from ShB. *Science.* 250:568–571. http://dx.doi.org/10.1126/science.2122520

Zagotta, W.N., N.B. Olivier, K.D. Black, E.C. Young, R. Olson, and E. Gouaux. 2003. Structural basis for modulation and agonist specificity of HCN pacemaker channels. *Nature.* 425:200–205. http://dx.doi.org/10.1038/nature01922

Zhou, M., J.H. Morais-Cabral, S. Mann, and R. MacKinnon. 2001. Potassium channel receptor site for the inactivation gate and quaternary amine inhibitors. *Nature.* 411:657–661. http://dx.doi.org/10.1038/35079500

Zhou, Z., Q. Gong, B. Ye, Z. Fan, J.C. Makielski, G.A. Robertson, and C.T. January. 1998. Properties of HERG channels stably expressed in HEK 293 cells studied at physiological temperature. *Biophys. J.* 74:230–241. http://dx.doi.org/10.1016/S0006-3495(98)77782-3